Fluorescence diagnosis and photochemical treatment of diseased tissue using lasers: Part II

Andersson-Engels, Stefan; Johansson, Jonas; Svanberg, Katarina; Svanberg, Sune

Published in:
Biochim. Clin.

DOI:
10.1021/ac00200a001

1990

FLUORESCENCE DIAGNOSIS AND PHOTOCHEMICAL TREATMENT OF DISEASED TISSUE USING LASERS: PART II

Stefan Andersson-Engels, Jonas Johansson, and Sune Svanberg
Department of Physics
Lund Institute of Technology
P.O. Box 118
S-221 00 Lund
Sweden

Katarina Svanberg
Department of Oncology
Lund University Hospital
S-221 85 Lund
Sweden

In this two-part series, Sune and Katarina Svanberg and co-workers focus on the spectroscopic aspects of laser use in several emerging applications of medical importance. Part I, which appeared in the December 15 issue (1), *surveyed laser techniques for atomic and molecular analyses of samples of clinical interest, spectroscopic analysis of the laser-induced plasma obtained when a high-power pulsed laser beam interacts with tissue, and the use of tumor-seeking agents in combination with laser radiation to provide new possibilities for malignant tumor detection and treatment.*

In Part II, we describe the use of laser-induced fluorescence (LIF) for tumor and plaque diagnostics. The diagnostic potential is increased by including the temporal characteristics of the fluorescence decay. The extension of point monitoring to imaging measurements also is described, together with implications for practical clinical work.

Tumor diagnostics using LIF

LIF studies are performed in a laser regime where no change in the tissue is induced. The photon energy is chosen sufficiently below the limit for DNA photodissociation to avoid mutagenicity.

LIF has proven to be useful for diagnostic purposes, and early work was reported by American (*2*, *3*) and Chinese (*4–6*) groups as well as by our research group (*7*, *8*). The ground state and the first excited electronic levels of large molecules such as biological ones are broadened by vibrational motion and interactions with surrounding molecules. Thus, absorption occurs in a broad band, allowing a fixed-frequency laser such as the nitrogen laser (λ = 337 nm) to be used for the excitation. A radiationless relaxation to the bottom of the excited band then occurs on a picosecond time scale. The molecules remain here for a typical lifetime of a few nanoseconds. Fluorescent light is released in a broad band, which does not normally exhibit any sharp features. Intersystem crossing to the triplet state, internal conversion, and the transfer of energy to surrounding molecules are strongly competing radiationless processes. Tissue containing hematoporphyrin derivative (HPD) molecules will exhibit sharp spectral features in the red spectral region.

In exploiting tissue LIF for medical diagnosis, it is useful to start with detailed laboratory studies of tissue samples. In most of our studies, a N_2 laser emitting 5-ns pulses at 337 nm has been employed for excitation; a XeCl excimer laser (λ = 308 nm) and an excimer-pumped dye laser have also been used. The radiation is directed onto the sample by mirrors. Fluorescent light is collected and directed to an optical multichannel analyzer system that

INSTRUMENTATION

0003-2700/90/0362-019A/$02.50/0

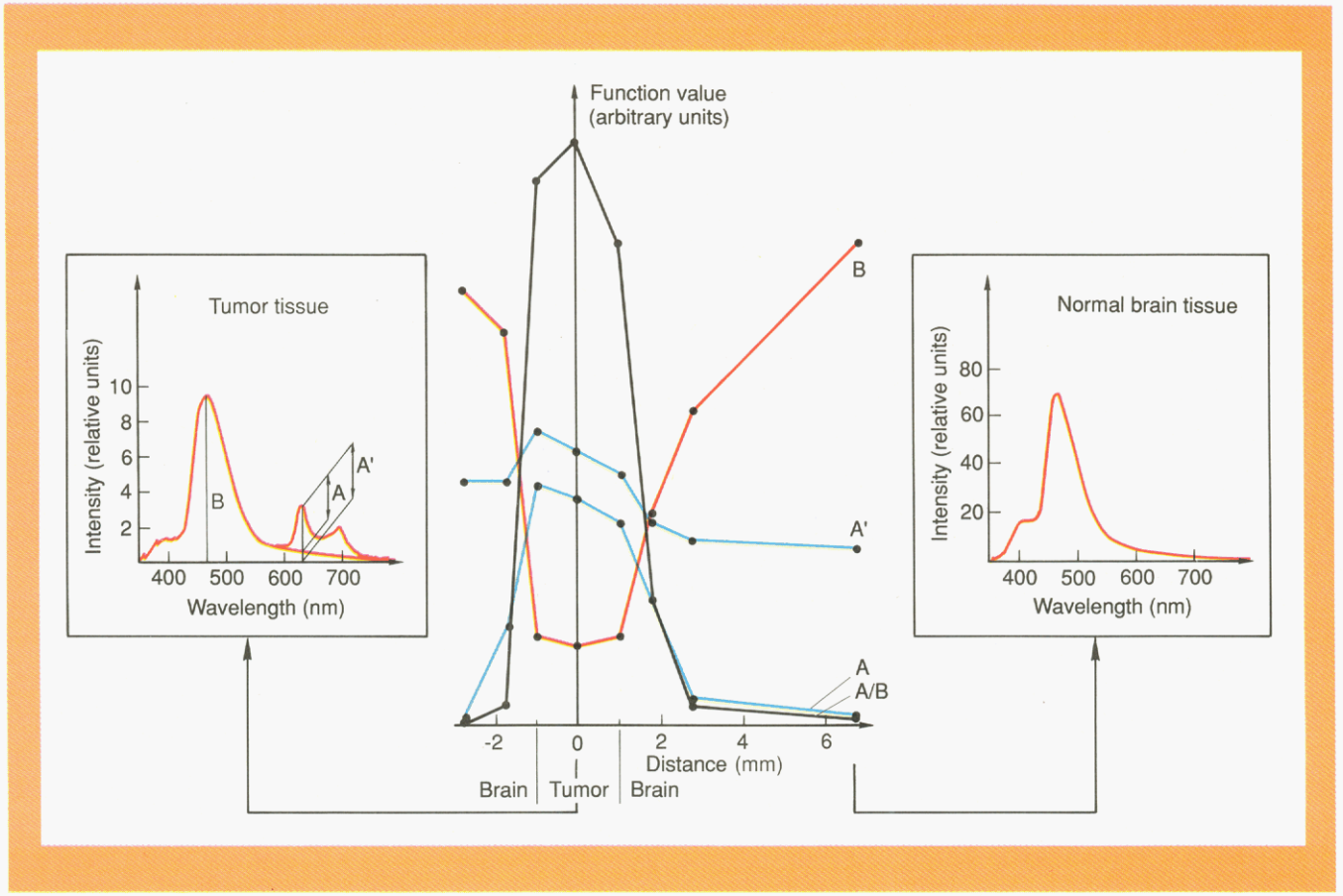

Figure 1. Fluorescence data obtained with 337-nm excitation in a scan over a tumor in the brain of a rat that received 1 mg/kg body weight Photofrin II (dihematoporphyrin ether/ester) prior to the investigation.

Left: Fluorescence spectrum of the central tumor is shown with fluorescence intensities A, A′, and B. Right: Fluorescence spectrum of the nonaffected normal surrounding brain tissue. Note the different intensity scales. Functions of the fluorescence intensities along the scan are presented in the center. (Adapted with permission from Reference 10.)

captures the entire fluorescent light distribution for every laser pulse. The system incorporates a gated image-intensified diode array detector that is placed in the focal plane of the small spectrometer. The detector gating, normally set to 500 ns, makes it possible to suppress continuous background light while collecting all fluorescent light. Spectra can be stored on floppy disks and printed out on paper. Fluorescence intensities are measured according to a standard.

For clinical fluorescence studies we have used a similar system that is equipped with a fiber-optic probe. Light from a N_2 laser or a dye laser pumped by the fixed-frequency laser is focused into 600-μm-diameter quartz fibers via a dichromic beam splitter that reflects the UV light but transmits all visible radiation. Fluorescent light from the sample is collected by the same fiber and is directed to the entrance slit of the optical multichannel analyzer system. The fiber can be inserted through the biopsy channel of an endoscope for investigations of corpular lumina (*9*).

As a first illustration of tissue diagnostics, data from a fluorescence scan through an experimental malignant brain tumor in a rat are shown in Figure 1 (*10*). The animal received an injection of dihematoporphyrin ether/ester (DHE) corresponding to 1 mg/kg body weight before the investigation. The recorded spectrum on the left shows a clear signature of DHE in the 600–700-nm wavelength region that was obtained using 337-nm excitation. In the right-hand part of the figure, the HPD signal is absent in normal brain tissue. In addition, the bluish autofluorescence is strongly reduced in the malignant tumor tissue.

To display these observations more quantitatively, the intensity at 630 nm was evaluated as the signal A′. By subtracting the background, we obtain the intensity A; the blue fluorescence intensity at 470 nm is denoted by B. In the plot the strong contrast enhancement obtained by using the background-free intensity A is demonstrated, and the decrease in the autofluorescence intensity is clearly displayed. By forming the ratio A/B, contrast can be further improved, as illustrated in Figure 1. Such a ratio forms a dimensionless quantity, which has the attractive feature of being independent of surface topography and variations in distance, excitation, and detection efficiency.

We have performed extensive studies in tissue fluorescence diagnostics in rats (*7*, *8*, *10–13*) to explore the effect of drug uptake and retention, tissue autofluorescence, and optimization of excitation wavelength. We have also compared the tumor-marking capability of different sensitizers. As an example, fluorescence spectra from tumors in rats injected with 15 mg/kg body weight are shown in Figure 2 for 337-nm excitation (*13*). An interesting feature of polyhematoporphyrin ester (PHE) is that the fluorescence peak is found further to the red compared with the other porphyrins. PHE is a highly aggregated and stable substance, whereas DHE still contains a substantial fraction of monomers. This might indicate that PHE is not converted to monomers in tissue, which is probably the case for DHE. This theory is supported in the study of HPD using the

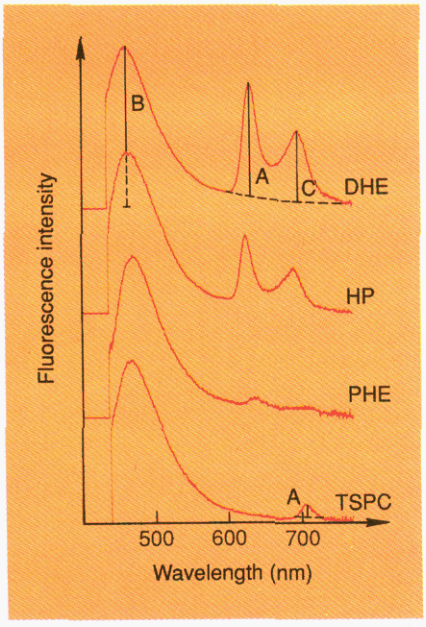

Figure 2. Typical LIF spectra (relative units) from rat tumors.

The rats were injected with 15 mg/kg body weight of hematoporphyrin (HP), dihematoporphyrin ether/ester (DHE), polyhematoporphyrin ester (PHE), and tetrasulfonated phthalocyanine (TSPC). The excitation wavelength was 337 nm. (Adapted with permission from Reference 13.)

HPLC method (illustrated in Part I of this series), where a fluorescence red shift was found for the more aggregated components.

Human tumor demarcation is illustrated by data from a fluorescence study of a metastasis of recurrent breast cancer (Figure 3). The patient received 2.5 mg/kg body weight of DHE one day before the study (*14*, *15*). Again, the tumor exhibited an increased red fluorescence and a decreased blue autofluorescence, which in combination yield a distinct tumor demarcation.

Plaque diagnostics using LIF

Atherosclerosis is another disease for which the use of laser light in diagnosis and therapy can have a great impact. Atherosclerosis can affect all kinds of arteries and most likely results from risk factors such as hyperlipidemia, hypertension, and smoking. The condition affects the endothelium cells at the surface as well as the underlying layer, the intima. A diseased region—a plaque—starts to develop with inclusions of different anomalies such as lipid droplets, cholesterol crystals, and

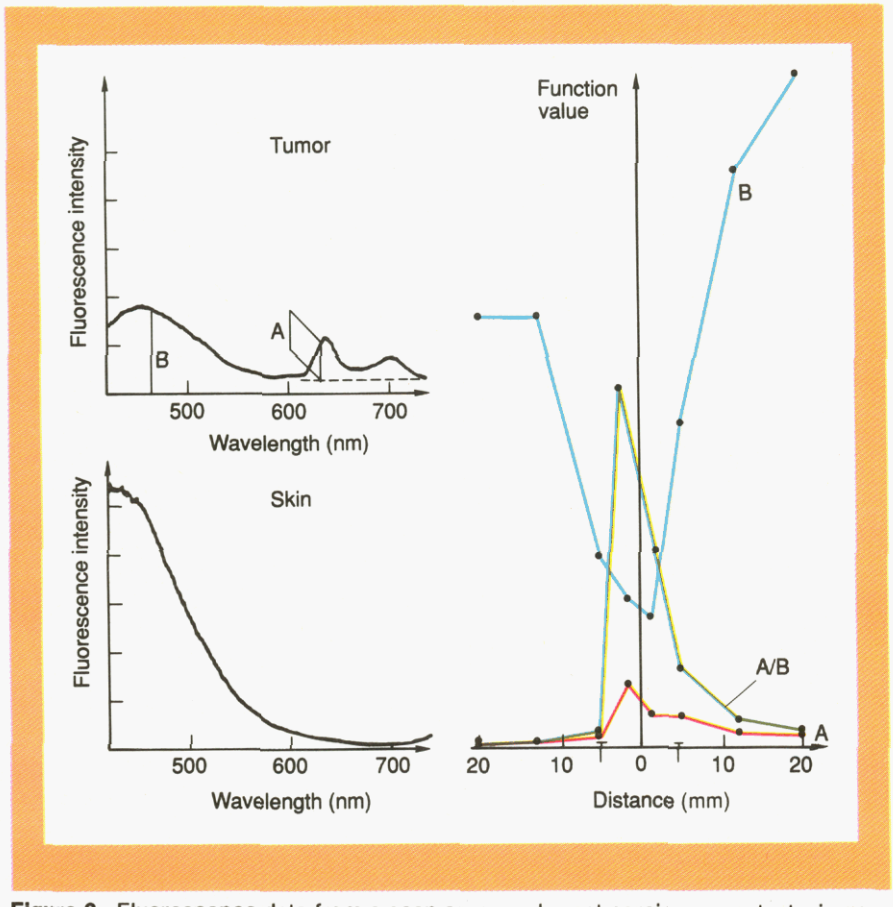

Figure 3. Fluorescence data from a scan across a breast carcinoma metastasis one *day after DHE injection.*

Sample spectra for tumor and surrounding tissue are shown with evaluated fluorescence intensities. The drug dose was 2.5 mg/kg body weight. (Adapted with permission from Reference 15.)

calcifications (Figure 4). The surface of the lesion consists of fibrotic constituents such as collagen and elastin. The pigment β-carotene is also present in plaques. When the damage has reached a serious level, calcification also occurs at the surface and the endothelium is severely disrupted, with the potential for thrombosis formation.

The removal of plaque in diseased or obstructed vessels by laser radiation administered through a fiber-optic light guide (laser angioplasty) is an extremely attractive possibility (*16*, *17*). However, the risk of vessel perforation presents a serious problem, and improved diagnostics are needed to ensure that the fiber tip is placed at the correct location within the vessel. An interesting task is to try to spectroscopically distinguish atherosclerotic plaque from normal vessel tissue.

The first fluorescence experiments aimed at spectroscopic guidance in laser angioplasty were reported by Kittrell et al. (*18*), who used excitation at 480 nm. We find that by using N_2 laser excitation at 337 nm, prominent differences between atherosclerotic plaque and normal artery wall can be found in fluorescence spectra—for both large vessels, such as the aorta and pulmonary arteries, and small ones, such as coronary vessels (*19*, *20*). Examples of spectra can be found in Figure 5 (*19*). The intensities at 390, 415, 480, 580, and 600 nm are evaluated as signals a, b, c, d, and e, respectively. We have experimented with different dimensionless contrast functions to obtain good discrimination between plaque and normal tissue. As can be seen from the fluorescence scan shown in the figure, ratios such as a/c and b/c discriminate well between plaque and normal artery wall, whereas d/e does not.

Fluorescence studies of arteries have been performed by several groups using different excitation wavelengths (*21–24*). Most of the studies have been performed in vitro. The data shown in Figure 5 are obtained from a resectioned and rinsed segment of a human artery. Although superficial blood is removed, the spectra show clear signs of hemoglobin reabsorption at 415, 540, and 580 nm. Clearly, varying amounts of blood between the tissue and the

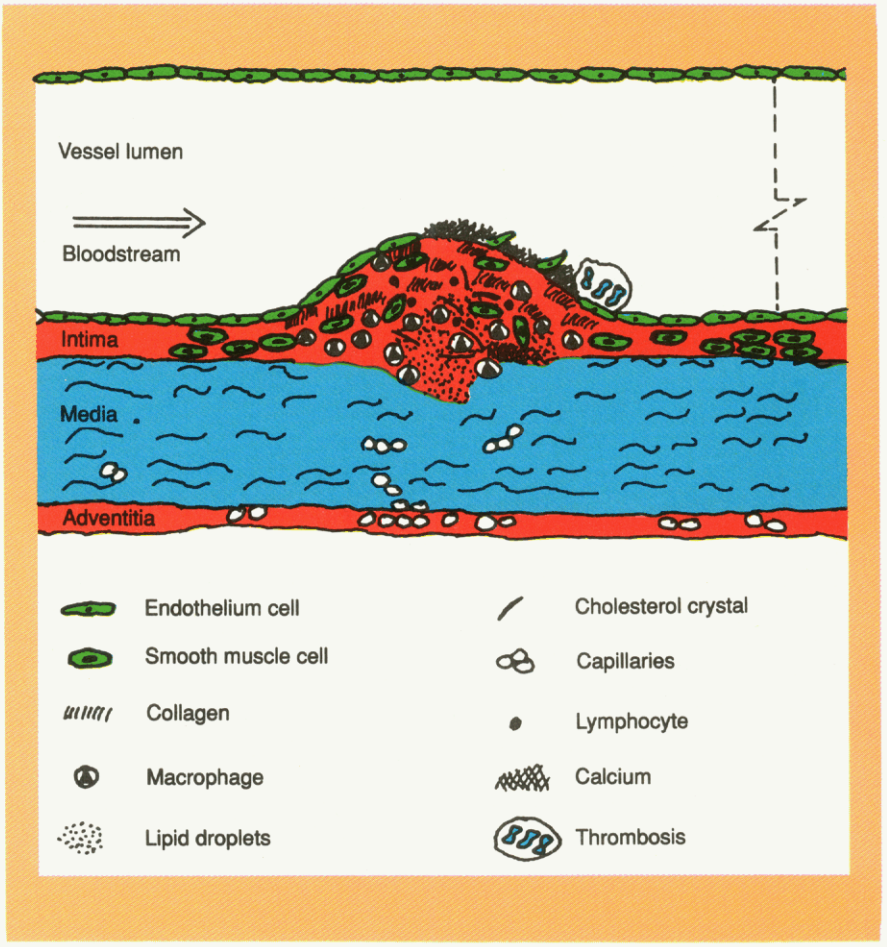

Figure 4. Illustration of a cross section through a blood vessel with an atherosclerotic plaque.
A thrombosis is under development on the downstream side of the plaque.

measurement fiber could strongly affect the spectral characteristics of the fluorescence spectrum. Thus, for reliable clinical applications, the plaque identification criteria must be largely independent of blood.

One way to achieve this is to evaluate the fluorescence intensities at two wavelengths where the blood absorption is the same, so that the blood interference is eliminated when a ratio of the absorptions is formed (*19*, *25*). Such a wavelength pair is 380 and 437 nm. Another possibility is to use the temporal characteristics of the fluorescence decay. We have recently shown that the signal attributable to plaque has a longer decay time than normal nondiseased vessel wall, as illustrated in Figure 6a (*26*). A synchronously pumped dye laser was cavity dumped, and the 6-ps pulses were frequency doubled to 325 nm in these studies. The lifetimes are actually long enough to allow the use of a N_2 laser with 3-ns pulses in conjunction with a dual-channel boxcar integrator, as illustrated in Figure 7 (*25*). The gate of one channel is set for "late" fluorescence (5–15 ns) and the other is set for "early" fluores-

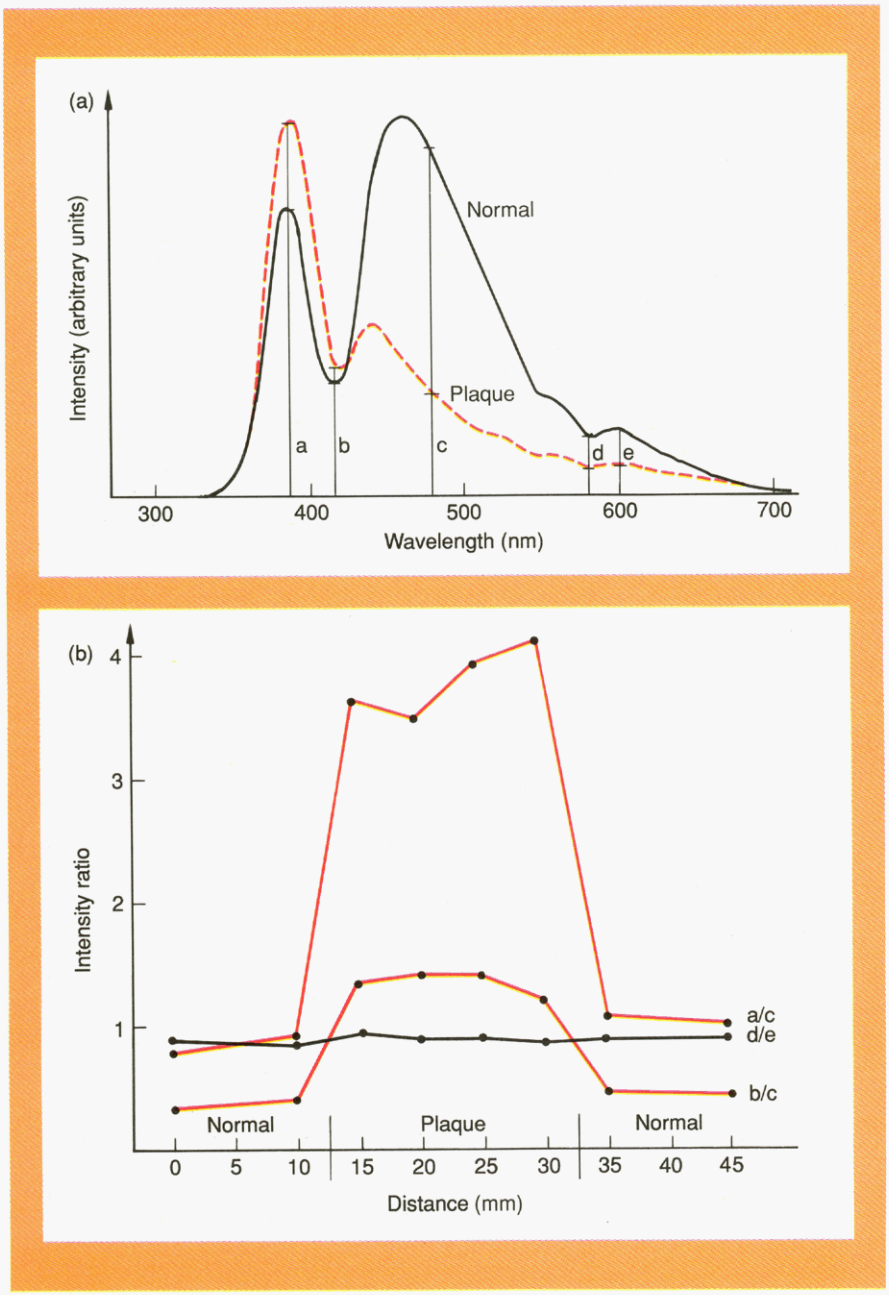

Figure 5. Fluorescence spectra of normal and atherosclerotic aorta.

(a) The fluorescence intensities at five different wavelengths—390, 415, 480, 580, and 600 nm (a–e)—are indicated. (b) Scan through an atherosclerotic plaque region with data from three dimensionless contrast functions displayed. The excitation wavelength was 337 nm. (Adapted with permission from Reference 19.)

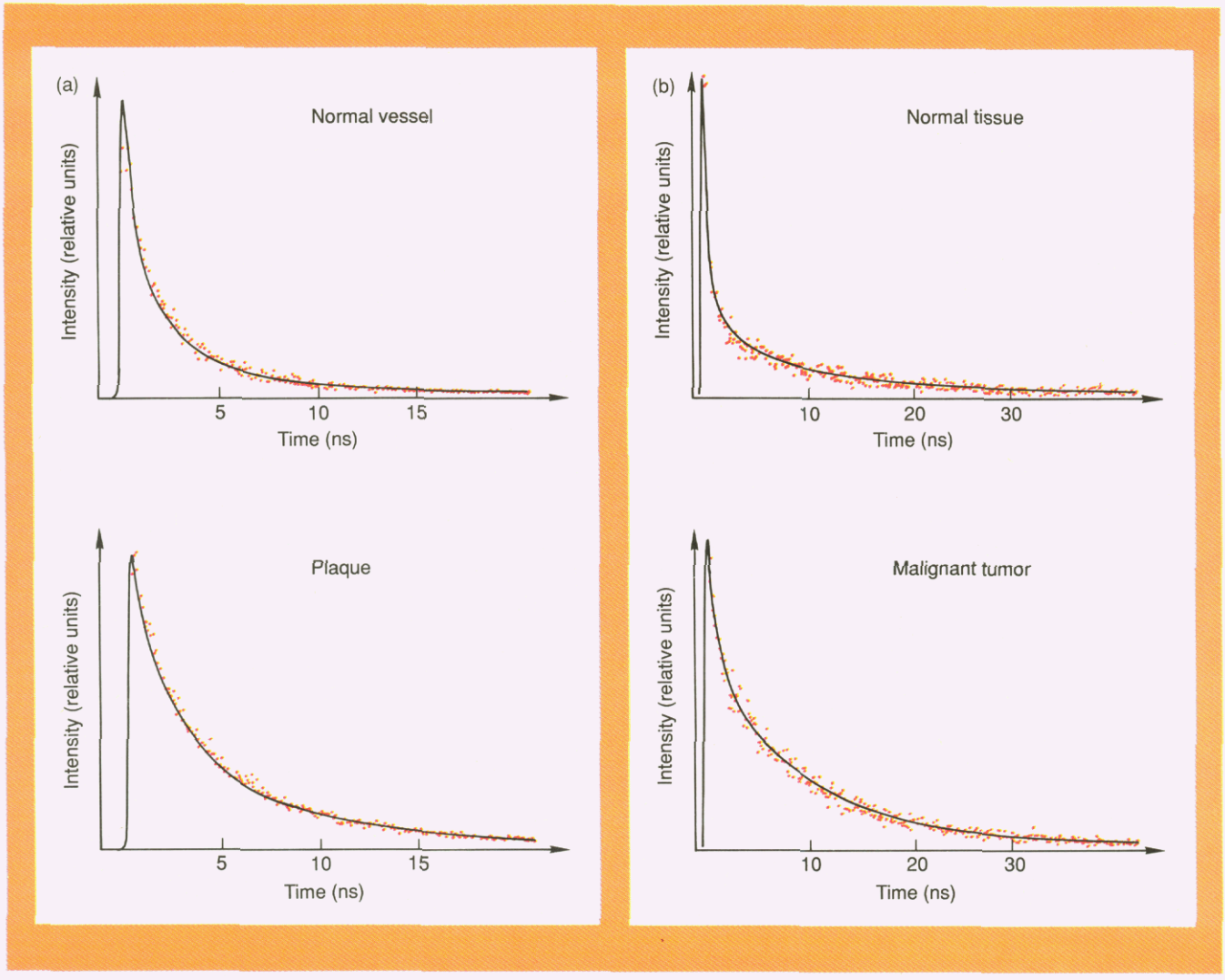

Figure 6. Fluorescence decay curves of (a) a normal blood vessel and an atherosclerotic plaque as well as (b) normal muscle tissue and a malignant tumor.

The excitation wavelength was 325 nm. Emission wavelengths were (a) 400 nm and (b) 630 nm. The colon adenocarcinoma tumor was subcutaneously grown on the hind leg muscle of a rat injected with 15 mg/kg body weight of DHE.

cence (0–5 ns). By dividing the signals, a higher value is obtained for the slowly decaying plaque fluorescence than for the normal wall.

In Figure 7, the different tissue types can be readily identified when the fiber-optic probe is moved from spot to spot. Because the detection is performed at a single wavelength (400 nm) for which light absorption has a higher cross section than scattering in blood, and because the blood is nonfluorescing, the blood acts only as a passive light attenuator and does not influence the fluorescence decay.

Time-resolved fluorescence monitoring using porphyrin localizers is another way to achieve enhanced tumor detection. The HPD fluorescence at 630 nm has a longer decay time than the autofluorescence background at the same wavelength, as illustrated in Figure 6b for the case of the rat tumor (*27*). Thus, by gating the detection system for late fluorescence, the HPD signal can be recorded background free.

Point monitoring for clinical work, aimed particularly at HPD-assisted tumor detection, has been constructed. Filter spectrometers (*28–30*) and optical multichannel detection (*31–32*) have been employed.

Fluorescence imaging

Medical imaging based on computerized X-ray and NMR tomography has recently reached an advanced state of development. Clearly, fluorescence imaging systems with contrast enhancement as discussed above would be of considerable interest. However, normally one must make a choice between monitoring the whole LIF spectrum at one point and monitoring a spatial region in one fluorescence band. Using special optical arrangements and employing contrast functions of the type discussed above, an interesting combination of these two possibilities can be achieved (*33*). We will describe the development of a multicolor imaging system now under way in our laboratory (*34, 35*).

To obtain spatial and spectral resolution simultaneously, we divide the fluorescence light with a multimirror arrangement, as shown in Figure 8 (*25*). The object is illuminated with a UV light source, which may be a laser or a flashlamp. Using a spherical mirror divided into four individually adjustable parts, it is possible to arrange four identical images as quadrants in an intensified matrix detector (charge-coupled device, or CCD detector). An interference filter arrangement in front

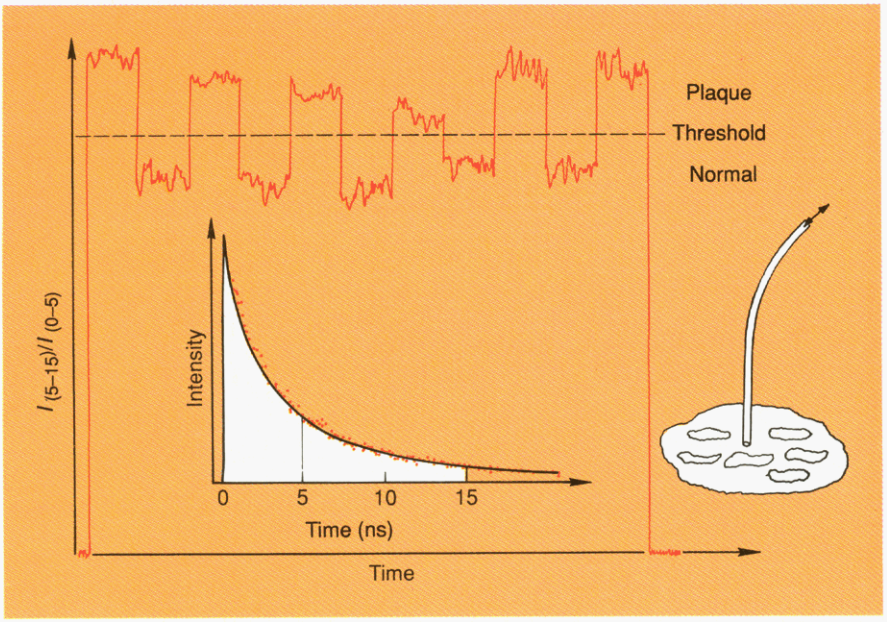

Figure 7. Time-resolved fluorescence measurement on the ratio of "late" to "early" fluorescence in a scan through a plaque region.

The excitation and emission wavelengths were 337 and 380 nm, respectively. The fluorescence light was guided through an optical fiber to a photomultiplier tube. The time gating and signal division were obtained in a boxcar integrator. (Adapted with permission from Reference 25, © 1990 IEEE.)

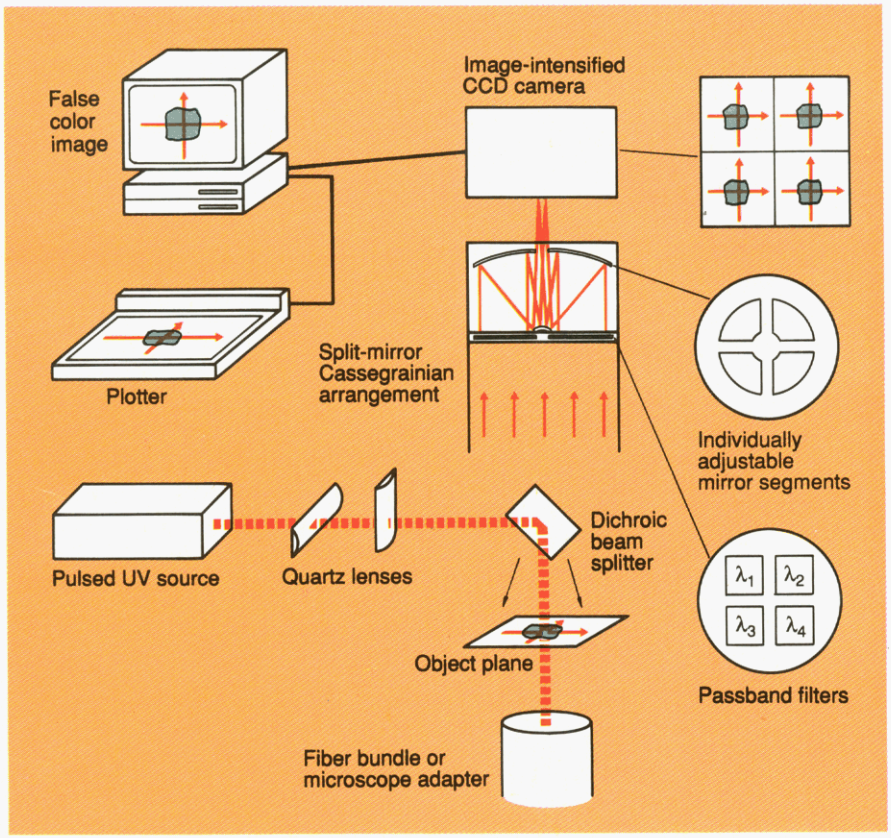

Figure 8. Arrangement for multicolor fluorescence imaging.

(Adapted with permission from Reference 25, © 1990 IEEE.)

of the split mirror is used to filter out individual transmission bands for the four images. From the four images a dimensionless contrast function is calculated for each spatial location using the corresponding pixel values in the fluorescence images. Finally, a generalized image that spatially displays the contrast function is formed. By choosing suitable passband filters based on

point measurements of the full spectral distribution, as discussed above, and by forming the relevant function to optimize contrast, tissues can be imaged with a contrast far exceeding that obtained by individual spectral bands or visual inspection.

Our system incorporates a Delli-Delta image-intensified CCD camera and an IBM 386-compatible computer with a Data Translation Model DT 7020 vector processor (*35*). An example of the simultaneously recorded images is shown in Figure 9. When linear mathematical operations such as image subtraction are performed, a system calibration accounting for different detector efficiencies in two channels must be applied. For precision processing, imaging vignetting and geometrical distortions must be eliminated. The imaging correction information is provided by a well-defined fluorescent test image.

Modern microchannel plate image intensifiers are gateable down to at least 5 ns. Thus contrast can be further enhanced by combining images of early fluorescence with images of late fluorescence. As discussed above, this time response is sufficient to allow time-resolved imaging of plaque in a blood-free inspection field and for enhanced tumor demarcation.

Image equipment monitoring the fluorescence from a certain area in a given fluorescence band has been constructed by Profio and co-workers (*36*, *37*). Such instrumentation has also been used successfully for the detection of human bronchogenic tumors. In one construction, Profio and co-workers have demonstrated that background can be intermittently subtracted by switching to a blue-transmitting filter (38).

Future trends

Lasers in conjunction with fiber optics provide new and fascinating possibilities for the detection and treatment of human malignancies as well as heart and circulatory system diseases. Furthermore, discomfort that results from gallstones and kidney stones can be alleviated. Substituting simple fiber-optic procedures for traumatic major surgery is a challenge for doctors in collaboration with physicists.

Optical spectroscopy of laser-induced phenomena in tissue is rapidly increasing in importance. Fluorescence diagnostics of tissue has potential as a clinical aid both for localizing small occult malignant tumors and for ensuring proper surgical removal. It is important to use all information available in the spectral and temporal domains, particularly in the effort to keep the concentration of tumor-seeking agents at the lowest possible level to reduce light hypersensitization of the skin. New photosensitizers with attractive properties are being developed. Tissue autofluorescence also provides interesting possibilities for enhanced tumor localization and for plaque demarcation. In using autofluorescence, one must pay attention to eliminating the influences of strong and nonspecific chromophores, such as those in hemoglobin.

Point monitoring or imaging systems employing LIF also have important applications outside the field of medicine, where they were first used. Other applications include industrial (*39–41*) and environmental monitoring (*42*, *43*), combustion (*44–46*), semiconductor processing diagnostics (*47*, *48*), and forensic science investigations (*49*).

This work was supported by the Swedish Cancer Society (RmC), the Swedish Board for Technical Development (STU), and the Knut and Alice Wallenberg Foundation.

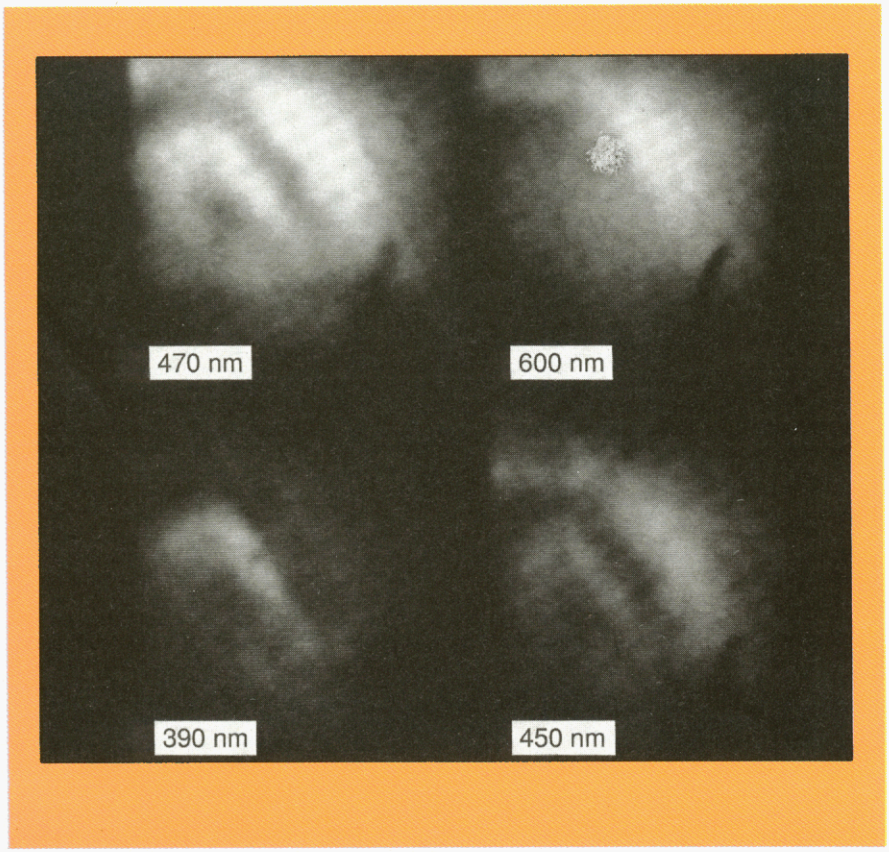

Figure 9. Two-dimensional fluorescence image of an aortic sample with an atherosclerotic plaque in the lower left corner.

The image was obtained using the experimental arrangement in Figure 8. The four detection wavelengths are indicated in the photograph. The darker line in the right lower corner is a thin metal wire. (Adapted with permission from Reference 25, © 1990 IEEE.)

References

(1) Andersson-Engels, S.; Johansson, J.; Svanberg, K.; Svanberg, S. *Anal. Chem.* **1989,** *61*, 1367 A.
(2) Alfano, R. R.; Darayash, B. T.; Cordero, J.; Tomashefsky, P.; Longo, F. W.; Alfano, M. A. *IEEE J. Quantum Electron.* **1984,** *20*, 1507.
(3) Alfano, R. R.; Tang, G. C.; Pradhan, A.; Lam, W.; Choy, D.S.J.; Opher, E. *IEEE J. Quantum Electron.* **1987,** *23*, 1806.
(4) Ye, Y.; Yang, Y.; Li, Y.; Li, F. *CLEO '85 Technical Digest*; Optical Society of America: Baltimore, MD, 1985; p. 84.
(5) Ye, Y.; Yang, Y.; Xia, J.; Li, F.; Li, Y. *Chinese Physics—Lasers* **1987,** 284.
(6) Yang, Y.; Ye, Y.; Li, F.; Li, Y.; Ma, P. *Lasers Surg. Med.* **1987,** *7*, 528.
(7) Ankerst, J.; Montán, S.; Svanberg, K.; Svanberg, S. *Appl. Spectrosc.* **1984,** *38*, 890.
(8) Svanberg, K.; Kjellén, E.; Ankerst, J.; Montán, S.; Sjöblom, E.; Svanberg, S. *Cancer Res.* **1986,** *46*, 3803.
(9) Andersson-Engels, S.; Elner, Å.; Johansson, J.; Karlsson, S.-E.; Salford, L. G.; Strömblad, L.-G.; Svanberg, K.; Svanberg, S. *Lasers Med Sci.*, in press.
(10) Andersson, P. S.; Kjellén, E.; Salford, L. G.; Strömblad, L.-G.; Svanberg, K.; Svanberg, S. *Lasers Med. Sci.*, in press.
(11) Andersson, P. S.; Kjellén, E.; Montán, S.; Svanberg, K.; Svanberg, S. *Lasers Med. Sci.* **1987,** *2*, 41.
(12) Andersson, P. S.; Ankerst, J.; Montán, S.; Svanberg, K.; Svanberg, S. *Lasers Med. Sci.* **1988,** *3*, 239.
(13) Andersson-Engels, S.; Ankerst, J.; Jo-

hansson, J.; Svanberg, K.; Svanberg, S. *Lasers Med. Sci.* **1989,** *4*, 119.
(14) Andersson-Engels, S.; Johansson, J.; Kjellén, E.; Killander, D.; Svaasand, L. O.; Svanberg, K.; Svanberg, S. *LIA ICALEO* **1987,** *60*, 67.
(15) Andersson-Engels, S.; Johansson, J.; Kjellén, E.; Killander, D.; Olivo, M.; Svaasand, L. O.; Svanberg, K.; Svanberg, S. *SPIE* **1988,** *908*, 197.
(16) Grundfest, W. S.; Litvack, F.; Forrester, J. S.; Goldenberg, T.; Swan, H.J.C.; Morgenstern, L.; Fishbein, M.; McDermid, S.; Rider, D. M.; Pacala, T. J.; Laudenslager, J. B. *J. Am. Coll. Cardiol.* **1985,** *5*, 929.
(17) Isner, J. M.; Steg, P. G.; Clarke, R. H. *IEEE J. Quantum Electron.* **1987,** *23*, 1756.
(18) Kittrell, C.; Willett, R. L.; de los Santos-Pacheo, C.; Ratliff, N. B.; Kramer, J. R.; Malk, E. G.; Feld, M. S. *Appl. Opt.* **1985,** *24*, 2280.
(19) Andersson-Engels, S.; Gustafson, A.; Johansson, J.; Stenram, U.; Svanberg, K.; Svanberg, S. *Lasers Med Sci.* **1989,** *4*, 171.
(20) Andersson, P. S.; Gustafson, A.; Stenram, U.; Svanberg, K.; Svanberg, S. *Lasers Med. Sci.* **1987,** *2*, 261.
(21) Cothren, R. N.; Hayes, G. B.; Kramer, J. R.; Sacks, B.; Kittrell, C.; Feld, M. S. *Lasers Life Sci.* **1986,** *1*, 1.
(22) Orayevski, A. A.; Letokhov, V. S.; Omelyanenko, V. G.; Ragimov, S. E.; Belyaev, A. A.; Akchurin, R. S. In *Laser Spectroscopy VII*; Persson, W.; Svanberg, S., Eds.; Springer: Heidelberg, 1987; p. 370.
(23) Sartori, M.; Sauerbrey, R.; Kubodera, S.; Tittel, F. K.; Romperts, R.; Henry, P. H. *IEEE J. Quantum Electron.* **1987,** *23*, 1794.
(24) Deckelbaum, L. I.; Sarembock, I. J.; Stetz, M. L.; O'Brien, K. M.; Cutrozzola, F. W.; Gmitro, A. F.; Ezekowitz, M. D. *Proc. SPIE* **1988,** *906*, Contribution 316.
(25) Andersson-Engels, S.; Johansson, J.; Stenram, U.; Svanberg, K.; Svanberg, S. *IEEE J. Quantum Electron.*, in press.
(26) Andersson-Engels, S.; Johansson, J.; Stenram, U.; Svanberg, K.; Svanberg, S. *J. Photochem. Photobiol.*, in press.
(27) Andersson-Engels, S.; Johansson, J.; Svanberg, S., unpublished work.
(28) Kinsey, J. H.; Cortese, D. A. *Rev. Sci. Instrum.* **1980,** *51*, 1403.
(29) Profio, A. E.; Doiron, D. R.; Sarnaik, J. *Med. Phys.* **1984,** *11*, 516.
(30) Andersson, P. S.; Karlsson, S.-E.; Montán, S.; Persson, T.; Svanberg, S.; Tapper, S. *Med. Phys.* **1987,** *14*, 633.
(31) Aizawa, K. et al. In *Porphyrin Localization and Treatment of Tumours*; Liss, A. R., Ed.; 1984, p. 227.
(32) Kato, H.; Cortese, D. A. *Clinics in Chest Medicine* **1985,** *6*, 237.
(33) Montán, S.; Svanberg, K.; Svanberg, S. *Opt. Lett.* **1985,** *10*, 56.
(34) Andersson, P. S.; Montán, S.; Svanberg, S. *IEEE J. Quantum Electron.* **1987,** 23, 1978.
(35) Andersson-Engels, S. A.; Johansson, J.; Svanberg, S. *Proc. SPIE* **1990,** 1205, Contribution 19.
(36) Profio, A. E.; Doiron, D. R.; Balchum, O. J.; Huth, G. C. *Med. Phys.* **1983,** *10*, 35.
(37) Profio, A. E. *Proc. SPIE* **1988,** *907*, 150.
(38) Profio, A. E.; Carvelin, M. J.; Sarnaik, J.; Wudl, L. R. In *Porphyrin in Tumor Phototherapy*; Andreoni, A.; Cubeddu, R., Eds.; Plenum: New York, 1984; p. 321.
(39) Montán, S.; Svanberg, S. *Appl. Phys.* **1985,** *B38*, 241.
(40) Montán, S.; Svanberg, S. *LIA. ICALEO* **1985,** *47*, 153.
(41) Andersson, P. S.; Montán, S.; Svanberg, S. *Appl. Phys.* **1987,** *B44*, 19.
(42) Measures, R. M. In *Analytical Laser Spectroscopy*; Omenetto, N., Ed.; Wiley: New York, 1984.
(43) Measures, R. M. *Laser Remote Sensing: Fundamentals and Applications*; Wiley: New York, 1984.
(44) Crosley, D. R.; Smith, G. P. *Opt. Eng.* **1983,** *22*, 545.
(45) Kychakoff, G.; Howe, R. D.; Hanson, R. K. *Appl. Opt.* **1984,** *23*, 704.
(46) Alden, M.; Edner, H.; Grafström, P.; Hertz, H. M.; Holmstedt, G.; Högberg, T.; Lundberg, H.; Svanberg, S.; Wallin, S.; Wendt, W.; Westblom, U. *Lasers 86*; STS Press: McLean, VA, 1985; p. 219.
(47) *Laser Diagnostics and Photochemical Processing for Semiconductor Devices*; Osgood, R. M.; Brueck, S.R.J.; Schlossberg, H. R., Eds.; North Holland: Amsterdam, 1983.
(48) Bauerle, D. *Chemical Processing with Lasers*; Springer: Berlin, 1986; Vol. I.
(49) Everse, K. E.; Menzel, E. R. *J. Forensic Sci.* **1986,** *31*, 466.